CLOUD SUPER-COOLED LIQUID WATER ESTIMATION FROM SATELLITE DATA

John K. Roskovensky[1], Mark Ivey[1], William Porch[2], Nick Beavis[1],
Ryan Herrmann[1], Sigmund Silber[3]

[1]Sandia National Laboratories, P.O. Box 5800, MS 0406, Albuquerque, New Mexico 87185

[2]Los Alamos National Laboratory, P.O. Box 1663, MS J577, Los Alamos, New Mexico 87545

[3]S. Silber and Associates, 22 B San Marcos Road E., Santa Fe, New Mexico 87508

Abstract. An automated algorithm for estimating the potential cloud super-cooled liquid water (SLW) from satellite data was developed to perform cloud surveys for assessing potential precipitation enhancement over the state of New Mexico. The algorithm produces spatial cloud SLW column distributions by utilizing many of the Moderate Resolution Imaging Spectroradiometer (MODIS) derived cloud products in addition to parameterizations developed to estimate vertical cloud thickness and fractional cloud liquid water content. Vertically derived cloud SLW is integrated to produce column totals. Algorithm uncertainties are assumed to be large, within a factor of two over the state of New Mexico, due to parameter sensitivity and high MODIS cloud water path uncertainties. Sensitivity studies identified differences up to 30% in SLW content from individual changes in the vertical cloud thickness estimation, moist adiabatic lapse rate, and cloud liquid fraction parameterization constants. Corrections of MODIS cloud water path artifacts also reduced the estimated SLW content by 10% to 50%. Comparisons of algorithm derived properties were made with other remotely sensed and *in situ* data. Algorithm cloud thicknesses were lower than co-registered CloudSat radar derived values by about 43% which likely led to an underestimation of liquid water content by more than 50%. Comparisons of the algorithm's vertical estimates of cloud SLW concentration to aircraft data during the Indirect and Semi-Direct Aerosol Campaign (ISDAC) in northern Alaska yielded consistent results. Ground based measurements from the Atmospheric Radiation Measurement North Slope Alaska site for seven days during ISDAC showed that the mean algorithm derived cloud base heights were nearly 1 km too high, but their adjusted temperatures were consistent with atmospheric sounding data. Algorithm derived SLW estimates were consistently within their uncertainty bounds in comparison with other measurements. Annual datasets from extreme dry and wet years over the state of New Mexico were examined to identify regions where cloud SLW appears prevalent and cloud seeding may be fruitful. Cloud SLW coincided well with high terrain especially in the Sangre de Cristo Mountains in the northern part of the state. Further analysis, focused on this specific region, found cloud SLW during the wet year to be 96% greater than in the dry year despite moderate (less than 20%) increases in all other cloud properties including cloud coverage, total cloud water, and cloud thickness. National Center for Environmental Prediction reanalysis data were sampled during these periods as well and during the wet year the number of days in which the 500 mb level wind was predominantly westerly increased by 12% along with an 8% increase in low-level humidity. Most of the annual difference occurred in the winter months. The parameters with the highest correlation to cloud SLW were the mid-tropospheric 700 mb to 500 mb level relative humidity. This analysis indicates that regions of potential cloud SLW may be very sensitive to subtle changes in environmental and cloud conditions.

1. INTRODUCTION

Knowledge of existing super-cooled liquid water (SLW) in clouds is important for cloud modification and precipitation enhancement. The primary objective of this study is to design and create a tool which interested parties could utilize to estimate the amount of possible cloud SLW from well calibrated satellite data combined with additional necessary and realistic cloud parameterizations. This tool or algorithm was intended to be used to define the relative distributions of cloud SLW from broad spatial and temporal examinations where intensive observations are not readily available thereby establishing preferred locations that might suit further, more comprehensive studies for realistic cloud seeding

*Corresponding author: John K. Roskovensky, Sandia National Laboratories, P.O. Box 5800, MS 0406, Albuquerque, New Mexico 87185; e-mail: jkrosko@sandia.gov.

activities. This allows us to survey regions and guide studies to answer questions such as:

1. How are certain regional clouds affected by environmental conditions, and
2. What large scale topographical forcing is most effective in increasing SLW and therefore the effectiveness of cloud seeding operations?

Small area efforts that rely on sizable ground instrumentation are best suited to study the effectiveness and directly aid active cloud seeding operations. Several efforts have been successful in this endeavor. Of particular significance to the mountainous state of New Mexico are orographic clouds. The four year Sierra Cooperative Pilot Project over the Sierra Nevada Mountains in California used a dual-band microwave radiometer to measure vertical distributions of cloud SLW in conjunction with detailed assessment of meteorological conditions in 63 wintertime storms (Heggli and Rauber, 1988). They were able to determine important characteristics of cloud SLW in terms of quantity, relative storm location, and cloud distribution with respect to the stage or development of the storm and its steering wind direction. Conditions favorable for precipitation enhancement were often observed with deep (greater than 500 m) ice saturation layers existing most often around -8°C to -10°C within 1 km of the surface as measured near the mountain crest. The recent Wyoming Weather Modification Pilot Project (WWMPP) focused on studying precipitation enhancement by employing randomized operations of several ground cloud seeding locations inside the two nearly-aligned Sierra Madre and Medicine Bow Mountain ranges in the south-central Wyoming (Boe, 2008). The region was instrumented with ground sensors including a dual-channel microwave radiometer deployed at various elevation pointing angles to perform orographic cloud measurement across a full spectrum of prevailing wind conditions. This effort was further supported by a nadir viewing aircraft mm-wave Doppler radar that could accurately sense cloud properties immediately above the surface at approximately 30 m (Geerts et al., 2010). Enhanced cloud reflectivity was measured downwind from operating ground cloud seeding generators which most likely resulted from increased ice particle concentration due to the introduction of ice nuclei. This enhancement was often observed strongly in cloud layers near the surface.

Satellite data alone cannot be used to fully predict where cloud seeding should spontaneously take place due to current limits in crucial three-dimensional microphysical property retrievals, spatial and temporal coverage, and derived product latency. The use of satellite data does offer routine broad area coverage of important cloud properties that can survey large regions and long time periods where little or no ground-based data are available. Algorithms previously developed to retrieve cloud water content from reflected sunlight (Han et al., 1998) and via microwave emission (Wentz, 1997) have been very useful and have been found to show consistent results in most cases (Horvath and Chellappan, 2009). The National Oceanic and Atmospheric Administration (NOAA) National Weather Service (NWS) has created an airline icing probability product (http://aviationweather.gov/adds/icing/) which attempts to determine the existence of cloud SLW in near real time from semi-persistent Geostationary Operational Environmental Satellites (GOES) data (Minnis et al., 2008). This algorithm utilizes the retrieved cloud top temperature, effective cloud particle size, and liquid water path to identify cloud regions with high water content, large cloud droplets, and cold temperatures that have a high probability for ice deposition. The technique has shown consistent results with pilot reports (PIREP) and may be useful for identifying regions where cloud seeding could be effective. The effects of cloud seeding have also been observed in satellite images of clouds. Xing et al. (2005) used exact knowledge of the position of a silver iodide cloud seeding aircraft along with modeled atmospheric transport, to match the zigzag flight pattern to enhanced visual effects in three-band synthesized Advanced Very High Resolution Radiometer (AVHRR) image with great accuracy. This cloud seeding maneuver affected the altostratus cloud top properties so that imbedded cloud tracks could be seen 20 to 80 minutes after seeding took place. Although it was not theorized why these enhanced image affects occurred, cloud tracks can stem from a higher than ambient number of cloud condensation nuclei (CCN) which increases the cloud reflectance due to more, but smaller cloud droplets (Twomey, 1977). The results of cloud seeding can also be identified by holes or canal like structures in clouds due to the removal of cloud droplets by precipitation. These affects are often seen in midlevel altocumulus cloud fields with an abundance of cold supercooled liquid water. If sufficient ice crystallization takes place through the introduction of seeding material falling from higher level cirrus, deliberate cloud seeding, or dynamical formation due to turbulence cloud liquid water can be lost through evaporation and subsequent ice deposition according to the Bergeron process. Heymsfield et al. (2010) presented several examples of modified holes in supercooled liquid water clouds as determined from both Moderate Resolution Imaging Spectroradiometer (MODIS) and GOES data. It was surmised that adiabatic expansion of air flowing around aircraft wing tips can produce cooling of as much as 20°C, causing some of the supercooled cloud droplets in this air to freeze with the resulting ice particles growing rapidly by the Bergeron process and precipitating out of the layer.

This paper presents a technique that utilizes common cloud data products from the space-based MODIS sensors to estimate potential cloud SLW. The algorithm described here was developed to survey and approximate the amount of cloud SLW that generally passes over the state of New Mexico during annual periods. Funding for this effort came from the New Mexico Small Business Assistance (NMSBA) program whose interested sponsors were keen to discover the extent of the water resources held in clouds that could be potentially precipitated to the ground through cloud seeding. This is needed in New Mexico and other regions where there is an absence of intensive cloud seeding studies. Establishing both spatial and temporal preferences of cloud SLW over the state was a primary focus. From this requirement, an algorithm was designed to characterize possible cloud SLW in clouds based on easily accessed horizontal cloud properties and reasonable assumptions of certain cloud vertical properties. It was not specifically designed to retrieve actual integrated cloud SLW via stringent assessment of actual cloud dynamic and microphysics. As a result, generalizations were used to ascertain key unknown cloud properties such as the vertical temperature and liquid water fraction profiles. Algorithm results were compared to derived products from data obtained by other sensors to show consistency, not absolute accuracy. To this extent, spatial, spectral, and temporal differences in the data were only taken into account by utilizing aggregation methods in order to smooth out sharp variations. These comparisons show that the algorithm produces results that are in general agreement to other measurements. Sensitivity analysis was made in order to expose the inherent response of the estimated cloud SLW on algorithmic assumptions as well as to approximate the algorithm uncertainty. It was found that varying cloud parameterizations by large, but realistic values altered the total cloud SLW by as much as 30%. The algorithm relies heavily on the derived MODIS cloud products of Cloud Water Path (CWP), Cloud Optical Depth (COD), and Cloud Top Temperature (CTT). Although the uncertainties in the latter two retrieved products are relatively small, the CWP uncertainty is often large with means around 30%, but is somewhat proportional to the magnitude of the retrieved CWP itself. Due to these input and algorithm uncertainties, the accuracy of the estimated cloud SLW content is likely within a factor of two. Linear artifacts in the CWP data were also noticed. A correction scheme is being developed to replace abnormally large cloud water values often seen as linear features. A more formal discussion of the algorithm is presented in the next section. The rest of this paper is a summation of the results obtained thus far which includes algorithm validation efforts with focus on consistency to other collocated data, and an assessment of estimated cloud SLW from two annual periods over the state of New Mexico. A summary is provided in the last section that also includes a description of future algorithm improvements and project efforts.

2. DATA AND METHODOLOGY

2.1 Algorithm Description

The Cloud Super-cooled liquid water Estimation Algorithm (CSEA) works in an automated fashion on key MODIS derived cloud properties and several input parameters. The derived MODIS products required are the Cloud Mask (CM), Cloud Optical depth (COD), Cloud Top temperature (CTT), Cloud Top Pressure (CTP), Cloud Water Path (CWP), and the Multilayer Flag. The derivations of these products are outlined in King et al. (1998) and Menzel et al. (2010). All of these products are defined at the 1 km band resolution with the exception of CTT and CTP, which are produced at 5 km. CSEA can run at spatial resolutions consistent with the 1 km data which may introduce an approximation error from the larger resolution products. Table 1 lists the important scientific parameters and their default values that were used in the algorithm to estimate cloud SLW. The Moist Adiabatic lapse rate (MALR) and atmospheric scale height values are set to mean global values. The maximum and minimum cloud SLW temperatures are given as 0°C and -40°C respectively, which is consistent with the generally accepted temperature limits in which SLW in clouds is expected (Heymsfield and Miloshevich, 1993). These can be set to more applicable values for cloud seeding such as -8°C to -20°C (Cooper and Lawson, 1984, and Cotton, 2009) if so desired. Temperature is not the only criteria for effective cloud seeding of course. Hygroscopic seeding particles that broaden the cloud droplet distribution can quicken the onset of precipitation formation (Cotton and Pielke, 1995). On the other hand, certain industrial aerosols have been shown to suppress precipitation (Rosenfeld, 2000). Therefore, the ambient aerosol type and size distribution near the clouds of interest, as well as those already inside the cloud acting as cloud condensation nuclei, would provide excellent ancillary information along with cloud SLW for potential cloud seeding effectiveness. MODIS does attempt to retrieve aerosol optical depth and size distribution parameters for cloud-free regions (Remer et al., 2006) that may be evaluated at the same time as cloud SLW. Unfortunately, the fidelity of the aerosol retrievals is limited over bright land surfaces (Remer et al., 2005) and the cloud-free aerosols may have little resemblance to the actual imbedded cloud aerosols. Finally, the minimum COD and maximum cloud top temperature parameters screen for thin clouds and warm clouds, respectively, which are then ignored by the algorithm.

Table 1. CSEA input parameters and their sensitivity on cloud SLW.

Parameter	Default Value
COD Minimum	1
Moist Adiabatic Lapse Rate	6°C/km
Maximum Cloud Thickness	Parameterized
Maximum Cloud Top Temperature	275 K
Minimum Cloud Base Height	500 m
Maximum SLW Temperature	273 K
Minimum SLW Temperature	233 K
Atmospheric Scale Height	7.6 km

Two versions of the algorithm exist, one set in satellite sensor space and the other that utilizes a gridding procedure. Since both employ the same methodology a discussion of the gridding procedures are ignored in this paper. CSEA assesses individual satellite pixels to produce a cloud SLW estimate. The initial criteria are a set of cloud tests. The algorithm assesses only pixels defined as confidently cloudy and of single-layer cloud by the MODIS cloud mask and multilayer cloud flag, respectively, with optical depth greater than the *COD minimum* parameter and a cloud top temperature less than maximum allowable cloud top temperature value. Any pixels which do not fit these criteria are skipped. The pixels that do fit these criteria are identified as cloud with potential SLW. There is currently no cloud typing test that includes the dominant phase of the cloud. A MODIS cloud phase product does exist but its reliability remains in question (Nasiri and Kahn, 2008). Other cloud phase algorithms have been developed which may aid in this task (Chylek et al., 2006, and Spangenberg et al., 2006a).

Further analyses of the potential cloud SLW pixels include the parameterization of their vertical properties starting with their physical thickness. A parameterization scheme for layered clouds from Minnis et al. (1995) is used in all cases for this initial version of the algorithm which defines vertical cloud thickness (Δz) as a function of COD and CTT according to the following criteria:

For CTT < 245 K, $\Delta z = 7.2 - (0.024 \cdot CTT) + (0.95 \cdot \ln COD)$

For CTT > 275 K, $\Delta z = 0.85 \cdot \ln COD$

For 245 K < CTT < 275 K, linearly interpolate Δz between 245 K and 275 K.

The left plot in Figure 1 shows parameterized cloud thickness values as a function of cloud top temperature for three cloud optical depths. For the same optical depth, cloud thickness increases with decreasing cloud top temperature. As optical depth increases for the same cloud top temperature, the estimated cloud thickness increases as one would expect. New cloud thickness estimations based on cloud type and phase may provide more accurate values (Chakrapani et al., 2002), but are not included presently because of the uncertainty in accurately characterizing the cloud type.

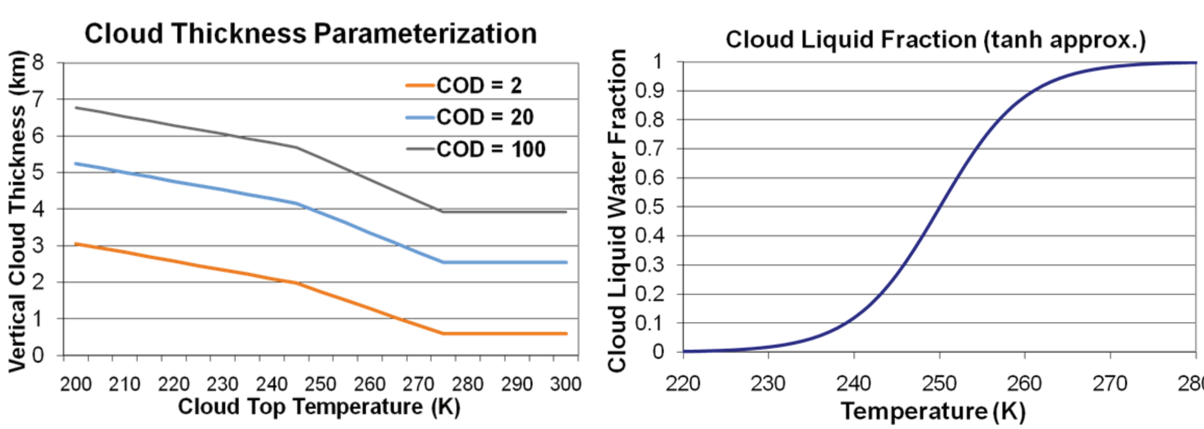

Figure 1: Parameterized cloud thickness for three COD values (left) and cloud liquid water fraction with temperature (right).

Cloud top and base heights are then calculated. A value for the cloud top height, *CTH*, is derived using the exponential pressure decrease curve with the atmospheric scale height, *H*, as follows:

$$CTH = -H^*(CTP/P_0).$$

P_0 represents mean sea level pressure, taken to be 1013 mb. The atmospheric scale height is assumed to be 7.6 km, which is consistent with the mean atmospheric temperature of 260 K. The cloud base is found by subtracting the parameterized cloud thickness from the cloud top height. A Digital Elevation Map (DEM) is included in the analysis to insure that the cloud base is not located below the ground level. In fact, if the cloud base is found to be lower than the *minimum cloud base height* parameter altitude mark with respect to the ground, it is set to an altitude equal to that threshold above the surface. The above ground default value of 500 m was used in these initial assessments due to the coarse 18.5 km resolution of the DEM employed in this version of the code, but this value could be lowered to the surface to evaluate specific low-level clouds often useful logistically in ground system cloud seeding operations (Huggins, 2009). The vertical temperature profile of the cloud is then derived using the globally averaged value of the MALR, a 6ºC linear increase in temperature for every kilometer decrease in height. Since the MALR is indirectly proportional to cloud water content and temperature, potentially more accurate MALR parameterization schemes based on these criteria are being investigated.

The final step consists of determining the fraction of the MODIS derived CWP that is in liquid form and within the commonly accepted SLW cloud region defined by the *maximum SLW temperature* (273 K) and the *minimum SLW temperature* (233 K) parameters. First, the MODIS derived CWP value is scaled by the percentage of the entire cloud thickness that has temperature residing inside the cloud SLW range since vertical cloud water is assumed to be constant. This assumption seems to be sound for shallow clouds up to 500 m in depth, but tends toward non-linear arrangements with local maximums due to internal dynamics for thicker clouds (Korolev et al., 2007). This resulting value is further scaled by the liquid water fraction inside the cloud SLW temperature range (e.g. the amount of liquid as opposed to ice). This liquid water fraction, X_{liq}, is parameterized as a function of temperature, *T*, by the following equation

$$X_{liq} = ½(1 + tanh(a_1{}^*T + a_2)),$$

where a_1 = 0.1 and a_2 = -25. These values were chosen to produce a 50% liquid water fraction at 250 K that gradually tails near 100% and 0% at the freezing point and -40°C, respectively. The liquid water fraction equation is graphical displayed in the right side graph in Figure 1. This parameterization of thermodynamic phase by a hyperbolic tangent function is of standard use in certain general circulation models and by the POLDER satellite-based algorithms that retrieve cloud phase (Doutriaux-Boucher and Quaas, 2004). The mean liquid water fraction of the cloud SLW region is found and used to scale the intermediate CWP value to determine the total cloud SLW column. This temperature-based parameterization of cloud liquid water was deemed acceptable in the absence of accurate microphysical property knowledge, but may be improved on in the future. Boudala et al. (2004) developed a cloud liquid water fraction parameterization from aircraft measurements of stratiform, clouds below freezing that is a function of both temperature and total cloud water itself. This scheme takes into account the liquid water fraction local minimum around -15°C where the maximum ice crystal growth based on vapor deposition is expected (Heymsfield et al., 1991).

An example of CSEA results from the MODIS sensor on board the Terra satellite on 6 October 2006 (1810 UTC) is presented in Figure 2. The true color image (top left) shows optically thick clouds along the western New Mexico border (outlined in red) with thin cloud cover over the majority of the central part of the state. The rest of the images only show the data fields over the New Mexico Area-of-Interest (AOI). The CTT and COD fields indicate there are high thin clouds diagonally arranged across the state with a high thick cloud region in the northwest corner. Warmer but optically thick clouds are seen along the middle part of the western border. Cloud water is derived in part from COD and thus mimics the COD field. The largest parameterized cloud thicknesses exist correctly for the clouds in the northwest corner but incorrectly for the thin cirrus in the middle of the state. This is the result of utilizing a layered, water cloud thickness parameterization scheme for all clouds. The only large cloud SLW region is seen in along the western border where the clouds were moderately warm (~250 K), optically thick, and possessed high water content. Low SLW values were estimated for the thick cold clouds in the northwest and the thin cirrus across the middle of the state. In both of these regions vertically thick clouds were parameterized, but their vertical temperatures did not correspond to high liquid water fraction sufficient to produce large amounts of SLW.

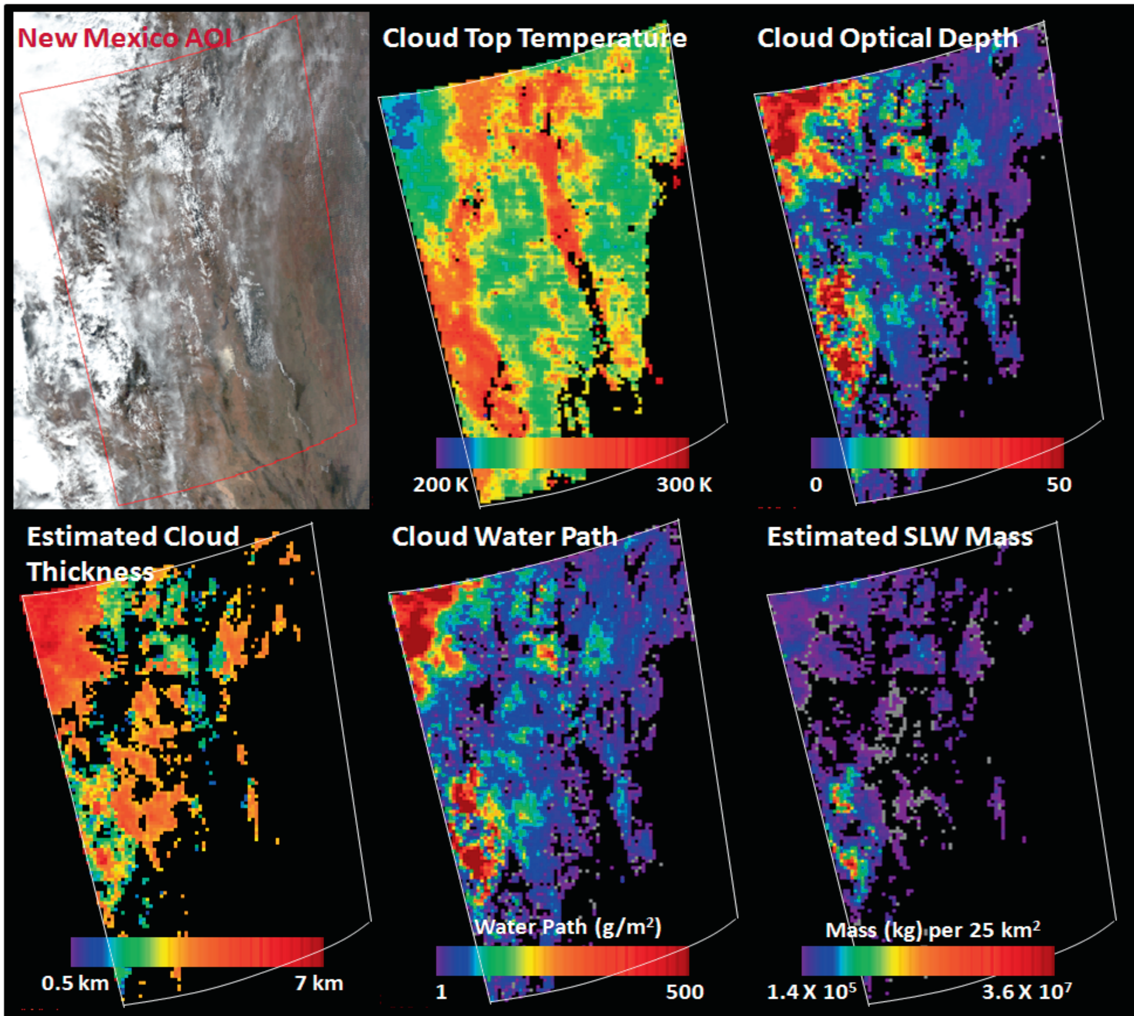

Figure 2: CSEA input cloud fields and estimated quantities from the MODIS (Terra) collection on 6 October 2006 (1810 UTC) over the state on New Mexico.

2.2 MODIS Cloud Water Path Dependence

The estimation of cloud SLW is directly dependent on the MODIS Cloud Water Path (CWP) product which quantifies the amount of cloud water in the satellite line-of-sight. CWP is derived from satellite data by the following equation

$$CWP = A*(4\rho_w/3Q_e(r_e))*\tau*r_e,$$

where, r_e is the effective cloud particle size, τ is the cloud optical depth, ρ_w is the density of liquid water, Q_e is the extinction efficiency, and A is a scale factor that is specific for ice or water particles (Chen et al., 2007). As such, this product is highly dependent on the prior retrieval of cloud optical depth and effective particle size as well as on the predominant cloud phase. Uncertainties in both cloud optical depth and effective particle size for water clouds are about 10% for optical depths less than 40 and particle sizes less than 25 microns, and larger for clouds with properties outside these criteria (Platnick et al., 2004). Mixed phase clouds do pose a problem since particle density and the scale factor are set according to a specific thermodynamic phase. From analysis of two annual periods over the state of New Mexico (discussed later) it was found that the mean and standard deviation of the CWP uncertainty for all detected clouds with COD greater than 1 was 30.8% and 18.3%, respectively. These uncertainties flow directly into the algorithm estimation of cloud SLW since the CWP values define the total cloud water.

It was also noticed that this product often possesses unrealistically large value linear artifacts in cloudy regions. These were suspected to stem from uneven calibration or processing aspects between the ten scanning detectors on the sensor. After some investigation the artifact appeared to be most pronounced in data from the Terra satellite while the Aqua satellite data seem somewhat free of this problem. A correction of these seemingly large false cloud water values was developed. The scheme initially identifies unnaturally high pixel values through comparison to pixels from adjacent scan lines in the satellite data space. These values are then replaced by more appropriate values from the adjacent scan lines. A visual example of the impact of this correction scheme is presented in Figure 3. A section of MODIS derived CWP on 1 February 2007 at 17:35 GMT from the Terra satellite is shown over the state of New Mexico in the left images. The yellow crosses correspond to the locations of Albuquerque and Santa Fe. High CWP linear artifacts are seen in both the top (state size) and, especially, in the bottom (zoom image) left most images. The largest CWP values (white) correspond to about 1800 g/m^2. The images on the right side of Figure 3 show that the high value linear artifacts in the corresponding corrected CWP fields have been somewhat removed.

MODIS CWP was compared to accurate ground radiometer measurements of liquid water in order to evaluate the derived satellite values and to verify the presence of SLW in some cases. A single case occurring over the Southern Great Plains (SGP) Atmospheric Radiation Measurement (ARM) site in northern Oklahoma provides an example. MODIS CWP on 31 January 2007 (1650 UTC) was compared to data from the Microwave Radiometer (MWR) and Infrared Thermometer (IRT) ground instruments. The three-day time series of the two instrument results are plotted in Figure 4. The approximate MODIS (Terra) overpass time at 1650 GMT on 31 January is highlighted by the small arrow on the horizontal axis. The IRT points vertically to measure sky temperature. When clouds pass over the instrument, temperature of the cloud near its base, which is much warmer than clear sky values, is measured. During the two day period from mid 31 January to early 2 February the sky was predominantly cloudy. The MWR can measure the cloud Liquid Water Path (LWP), shown in blue in the figure. Atmospheric water vapor measurements are also plotted in green. A good deal of cloud liquid water appears in conjunction with higher humidity (larger vapor values) from the middle of 31 January and persists until early 1 February. The cloud base temperature during this time is seen to fall just below freezing, and in supercooled liquid phase.

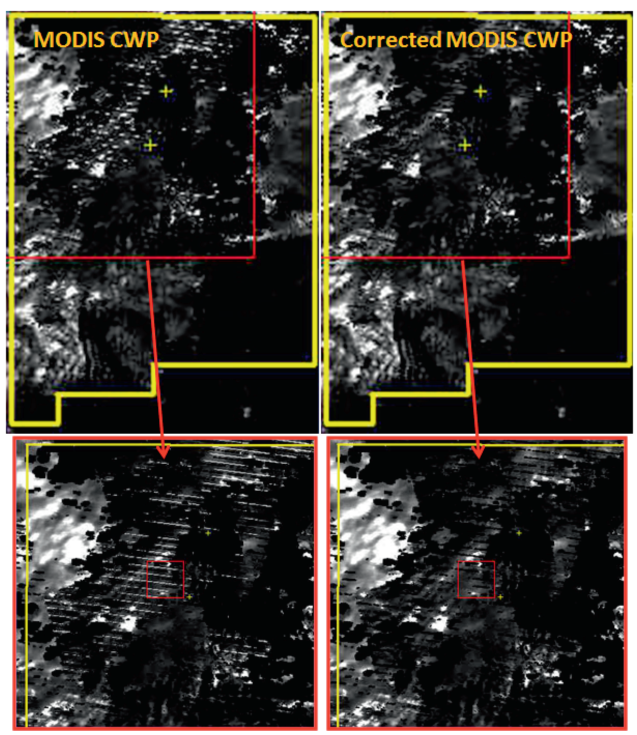

Figure 3: MODIS Cloud Water Path (left images) and the corrected field (right images) from the Terra Satellite over the state of New Mexico on 1 February 2007 at 17:35 GMT.

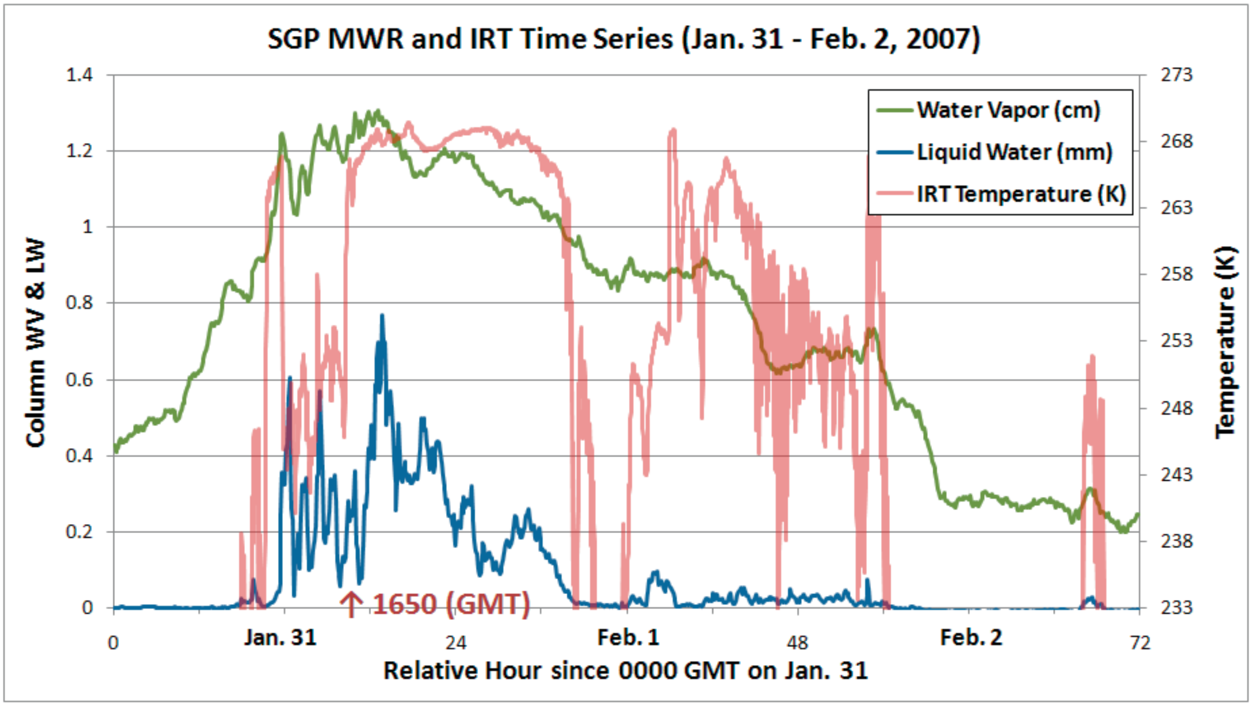

Figure 4: SGP IRT and MWR data are plotted for the 31 January to 2 February 2007 time period.

MODIS (Terra) CWP retrievals on 31 January 2007 (1650 UTC) are displayed in Figure 5. The patchy cloud field possesses between 200 g/m^2 (0.2 mm) and 600 g/m^2 (0.6 mm) of cloud water over the region near the SGP site. These values compare well with the 5-minute period mean MWR measurement of 0.29 mm centered on the satellite overpass. The mean IRT measured temperature was 264 K (-9°C) during that 5-minute period. At these temperatures the majority of the MODIS derived cloud water is expected to have been in super-cooled liquid form.

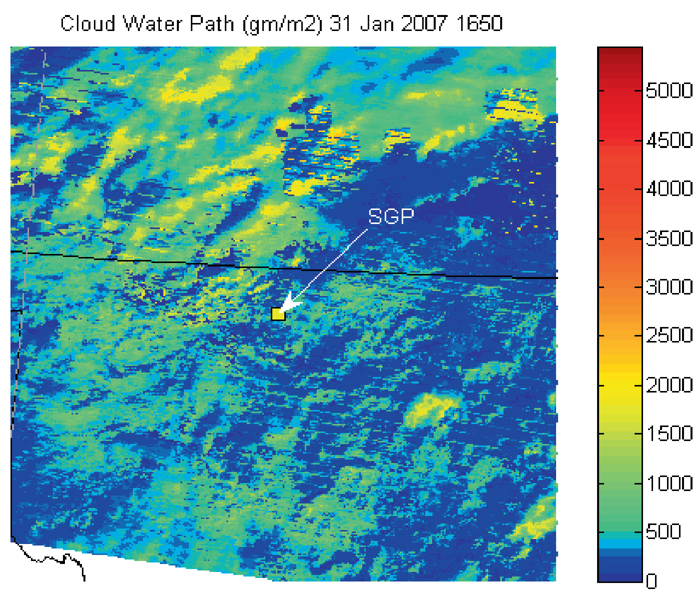

Figure 5: MODIS CWP over the SGP ARM site on 31 January 2007 (1650 UTC).

The CSEA algorithm is designed to provide best results for uniform stratiform clouds over flat terrain such as at the Oklahoma site described above. Deriving cloud liquid water over complex terrain and when broken clouds are present is a much greater problem. Figure 6 shows the results of the comparison of total cloud water derived from the MODIS sensor onboard the Aqua satellite to the liquid cloud water measured by microwave radiometers located at two locations in more complex terrain in the Upper North Platte River valley in Wyoming (Upper Cedar Creek and Savery). These measurements were taken during the WWMPP cloud seeding study during February 2008 and February 2009 (personal communication with Dan Breed). The 42 data points shown in the plot were selected when significant cloud liquid water was derived by MODIS and corresponding radiometer data were available. The most representative value for the radiometer data were used at the satellite overpass time. MODIS data products indicated that broken, non homogeneous clouds existed in most of these cases. Low cloud liquid water values measured with the radiometer were almost exclusively associated with cases where no satellite CWP value was determined and are not represented in the plot. Substantial difference exists between the derived satellite values and the ground measurements with MODIS CWP underestimating the radiometer measurements by 68.9%, especially in cases of high cloud water. This underestimation by the passive satellite products due to sub-pixel cloud variance or insensitivity to the lower reaches of thick, water laden clouds is apparent in this comparison and implies that, though the satellite product is useful as a survey tool for large regions and long data periods, it is not precise enough to quantify cloud liquid water at a specific location for cloud seeding studies.

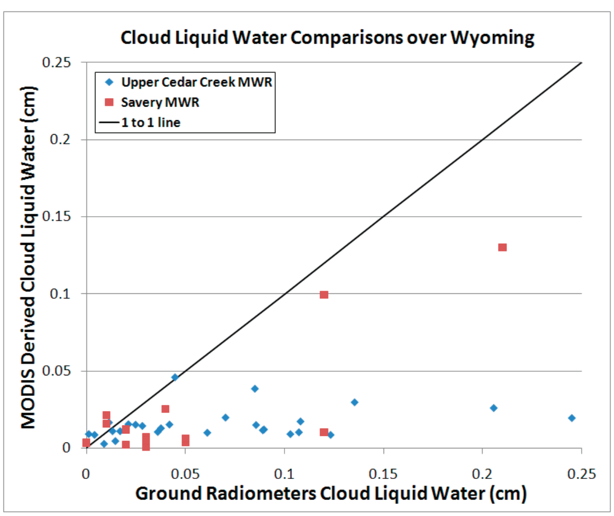

Figure 6: Comparisons of cloud liquid water measurements from two ground radiometers in Wyoming and collocated derived MODIS CWP values.

2.3 Sensitivity and Uncertainty

Table 2 lists the important parameters, their values, and their respective influence on the estimated cloud SLW. The specific sensitivity of the cloud SLW was determined by changing each individual parameter separately by the values listed in the second column during an assessment of 81 cloudy cases over New Mexico in the 14 month period from March 2006 to May 2007. Nearly 23 % of the potential cloud SLW appears to be in clouds with optical depths less than 5. It is understood that the estimate of cloud SLW is highly sensitive to the cloud temperature profile. Nearly 30% less SLW was calculated as the MALR was reduced to 2° C/km which marked the greatest change in cloud SLW. Limiting the parameterized cloud thickness to 4 km reduced the estimated mean cloud SLW by only about 11%, but a 2 km cloud thickness limit resulted in a 27.1% decrease in cloud SLW. A shift in the hyperbolic tangent liquid water fraction parameterization curve by +1 K lowered the cloud SLW content by 3.3%. A reduction of nearly one-quarter of the full-temperature cloud SLW total occurred as the minimum SLW temperature was increase by 20°C to 253 K. The effect of a constant atmospheric scale height was not examined. Altering the scale height would change the cloud top height slightly which could influence the cloud thickness. Since this overall resulting change in cloud thickness is expected to be small, the uncertainty due to a varying scale height is likely to be minor.

In an effort to define the algorithm cloud SLW estimation uncertainty the root mean square of the important approximated uncertainties was derived. From comparisons to other data sources (addressed later) parameterized cloud thicknesses were accurate to within 2 km which represented a 27.1% uncertainty. Since the MALR in clouds generally varies from 2°C/km to 10°C/km the use of a 6°C/km rate produces an uncertainty of 4°C/km, or 29.3%. Incorrect positioning in the parameterized cloud liquid water fraction curve leads to cloud SLW errors as well. An error of 5 K in position would lead to a 16.5% error in cloud SLW. The MODIS CWP uncertainty, defined by the mean and one standard deviation, during two annual periods over New Mexico ranged from 12.5% to 49.1%. The RMS value of the three algorithm affects along with the MODIS CWP was derived to range from 22.5% to 32.7%. It should be noted that this range in uncertainty is likely applicable only for this defined area and would have to be recalculated for other regions such as the arctic where MODIS CWP uncertainties appear to be much larger.

Table 2. CSEA input parameters and their sensitivity on cloud SLW.		
Parameter	**Value Change**	**Sensitivity**
COD Minimum	1 to 5	Decrease SLW mass by 22.8 %
Moist Adiabatic Lapse Rate	6 to 2 K/km	Decreased SLW mass by 29.3 %
Minimum SLW Temperature	233 K to 253 K	Decreased SLW mass by 24.5 %
Cloud Thickness	Parameterized to 2 km	Decreased SLW mass by 27.1 %
Liquid Water Fraction	Shift curve by +1K	Decreased SLW mass by 3.3%
Atmospheric Scale Height	7.6 km	Not Performed

3. ALGORITHM VERIFICATION

A limited number of comparisons with surface-based remote sensors, aircraft and space-based sensors were conducted to test the soundness of the algorithm results and are presented in this section.

3.1 Ground Measurements

Comparisons of CSEA derived cloud base height, adjusted cloud base temperature, and liquid water column were made with ground measurements over the North Slope Alaska (NSA) ARM site. Five minute data time series from the NSA ceilometer and the MWR as well as sounding temperature data provided true cloud base height, liquid water column, and estimated cloud base temperature, respectively. These were compared to mean algorithm derived properties of pixels identified to have passed over the ground site during the 5-minute interval using wind speed and wind direction from NCEP reanalysis data that most closely fit the ceilometer cloud base altitude. Table 3 lists the cloud property differences between the CSEA derived values and the respective ground measurements for seven days during the April 2008 Indirect and Semi-Direct Aerosol Campaign (ISDAC) field campaign. The adjusted CSEA cloud base temperatures are the values that were calculated at the true cloud base height by extrapolation with the MALR value of 6ºC/km. The differences between the adjusted algorithm cloud base temperatures and the measures of the true cloud base altitude temperature taken from the Point Barrow soundings at 12 Z is shown in the second numerical column of the table. These soundings, obtained from the University of Wyoming website (http://weather.uwyo.edu/upperair/sounding.html), were used because of the unrealistic sky temperatures seen in infrared thermometer (IRT) data.

Table 3. Cloud property differences of the CSEA results minus the ground measurements at the NSA-ARM site during seven days of the ISDAC field campaign.				
Date	**Cloud Base Height Difference (km)**	**Adjusted Cloud Base Temp Difference (K)**	**Cloud Liquid Water Difference (g/m2)**	**CSEA SLW Uncertainty**
4-Apr-2008	3.06	4.0	-19.2 (-87%)	199%
8-Apr-2008	-0.65	-2.1	15.1 (98%)	103%
14-Apr-2008	1.95	8.2	11.0 (182%)	173%
18-Apr-2008	1.20	9.9	19.8 (66%)	150%
19-Apr-2008	-1.17	1.5	-12.1 (-16%)	63%
24-Apr-2008	2.11	-5.2	No MODIS CWP Retrieval	
28-Apr-2008	0.02	10.3	-108 (-72%)	84%
Mean	**0.93**	**3.8**	**-15.5 (-7.6%)**	**102%**

The CSEA cloud bases were on average 930 meters higher than the ceilometer measurements. The algorithm parameterization seems to be underestimating cloud thickness (at least in the Arctic). Perhaps the correlation between the CSEA derived and actual cloud top heights is not perfect, which would create discrepancies in cloud base values. Ground-based derivations of cloud top properties have yet to be examined. At the same time, the adjusted CSEA derived cloud base temperatures compare well with the actual cloud base temperatures from the sondings. These small differences in cloud base temperatures indicate that the cloud temperature lapse rate in the algorithm appears accurate. All of the cloud base temperatures were measured to be below the freezing point of water which strongly suggests that the cloud liquid water was in the supercooled state. Mean algorithm estimated SLW was only slightly less than the mean MWR derived value even though daily differences varied substantially. The higher mean CSEA cloud base height could explain this difference. On the other hand, daily cloud base height errors did not correlate in sign with daily SLW errors (these should show a negative correlation). The reason for this is most likely due to the large associated SLW uncertainty that is passed on from the MODIS CWP product. As previously noted, this product relies on accurate cloud phase information which is difficult to obtain in the likely mixed phase clouds near the Arctic Ocean. It was found that about 90% of the clouds observed near NSA-ARM site during the Mixed-Phase Arctic Cloud Experiment (M-PACE) were of mixed phase (Spangenberg et al., 2006b). The daily SLW-MWR percentage differences are generally less than the inherent SLW uncertainties (last column in Table 3), which provides assurance that the CSEA estimates are reasonable.

3.2 Aircraft measurements

CSEA cloud property results were also compared to *in-situ* measurements from the Convair aircraft during the ISDAC over the north-slope of Alaska in April 2008. During the monthly campaign only two days provided sufficient comparisons when the aircraft was flying inside cloud boundaries defined by CSEA as the Aqua satellite passed overhead (April 5 and April 18). Both the algorithm and aircraft cloud liquid water and temperature retrievals are plotted in Figure 7. Due to the cold cloud temperatures, all liquid water is taken to be supercooled. CSEA SLW concentrations, derived by scaling the MODIS CWP per vertical distance by the parameterized liquid water fraction at the algorithm defined cloud temperature, compare well to aircraft liquid water measurements in both cases. The parameterized CSEA cloud temperature values were 2-3 K less than the aircraft measurements suggesting that either the cloud top height was incorrectly derived or the cloud MALR was slightly underestimated which would be consistent for colder polar clouds. These small temperature differences did not adversely affect the algorithm estimation of cloud SLW.

3.3 CloudSat

The CSEA cloud property results from 40 minutes of continuous MODIS data were compared to the corresponding clouds properties derived from CloudSat satellite radar data. CloudSat follows the MODIS sensor on the Aqua spacecraft by less than 1 minute and thus provides excellent comparisons of the same cloud with little expected change in its properties. This comparison of data from 64° S to 74° N contained many different cloud types associated with particular latitudinal zones. The MODIS

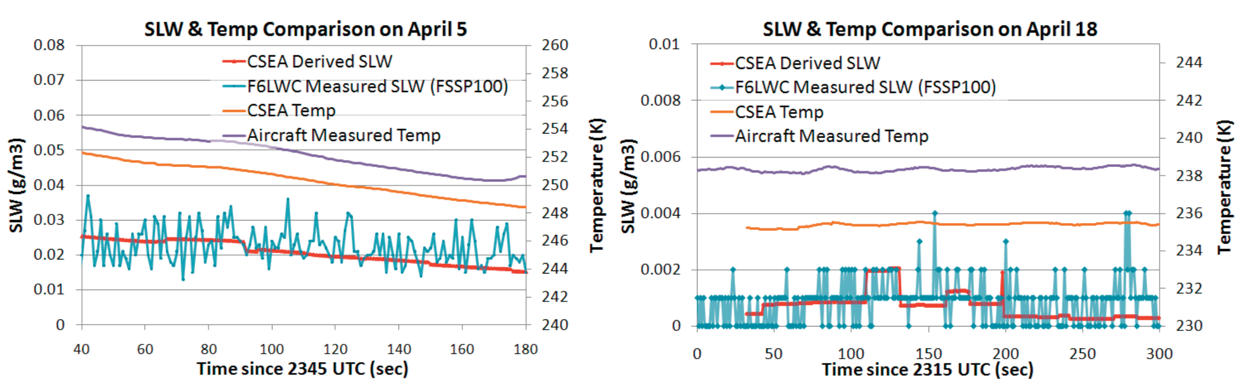

Figure 7: Comparison of CSEA derived and aircraft measured cloud SLW and temperature from the ISDAC field campaign.

CTT spatial fields (shown in the top image in Figure 8) give insight into the major cloud fields measured by CloudSat along its single line-of-sight approximated by the red arrow in the top image. The cold cloud tops correspond well to the high cloud tops shown in the middle graph of the figure. The CloudSat spatial footprint is about 1.7 km by 1.4 km. Comparisons were made by averaging the CloudSat data points that were contained in each corresponding 3 km x 3 km MODIS grid point. It can be seen that the CSEA cloud thicknesses are less than the CloudSat values for clouds with high tops, but the opposite is somewhat true for low-level clouds. Again, the cloud thickness parameterization is optimal for only moderately thick, layered clouds. CloudSat utilizes a 94-GHz radar which is fairly insensitive to cloud particles such that it can penetrate the entire thickness of the cloud and sense properties at all altitudes unlike passive sensors such as MODIS. This is likely the key contributor to the cloud thickness discrepancies between the two sensors. CSEA (MODIS) CWP values (bottom image) compare well to CloudSat values when the cloud thicknesses are similar.

The direct comparison of the mean value of four cloud properties from single-layer (SL) clouds identified by the separate datasets is shown in Figure 9. It is apparent that CSEA underestimates cloud top heights, cloud thickness, optical depth and cloud water path in comparison to the CloudSat derived values. Since cloud top temperature (a function of cloud top height) and cloud optical depth directly influence the parameterization of cloud thickness, lower cloud tops and optical depths could explain the 40% lower mean CSEA cloud thickness. Cloud Water Path (CWP) is proportional to both the effective cloud particle size and the COD. As a result, lower derived COD would naturally produce lower CWP values. Whether the 12% algorithm decrease in COD was primarily responsible for the 63% lower algorithm CWP values is not clear. It is also likely that relatively smaller cloud top particle sizes could have had a role in reducing the calculated CWP although this has yet to be investigated. In Arctic clouds, Liu et al. (2010) showed that CloudSat appeared to underestimate liquid water paths compared to ground-base MWR measurements likely due to the radar's liquid water path dependence on

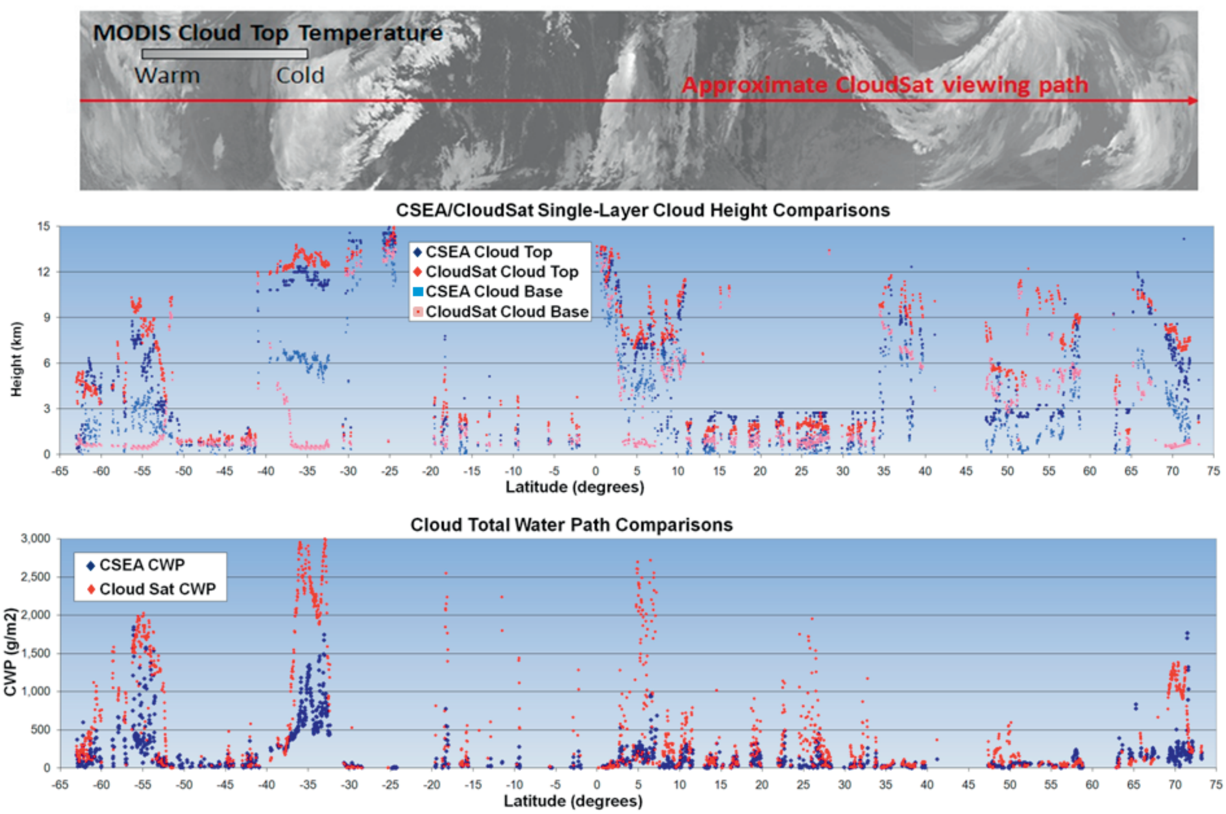

Figure 8: Spatial MODIS cloud top temperature (top) for 40 continuous minutes of data on 18 April 2008 (2240 – 2320 UTC), cloud vertical positions (middle) with single layer (SL) and multiple layer (ML) clouds noted, and CSEA and CloudSat derived CWP (bottom).

the smaller water cloud droplet radius (LWP ~ r^3) in mixed phase clouds. These comparisons indicate that CSEA may be underestimating cloud SLW which is uniquely tied to the cloud water path even though direct cloud SLW quantification was not directly contrasted.

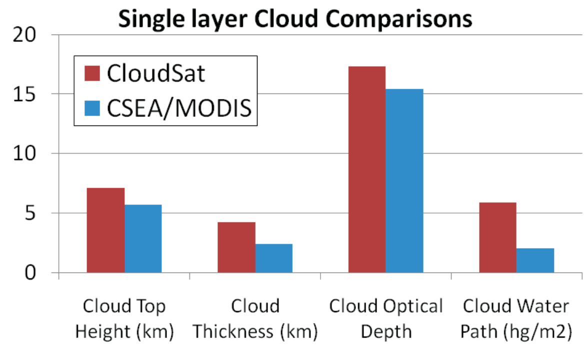

Figure 9: Results of single layer cloud comparisons from CloudSat and CSEA.

4. NEW MEXICO CLOUD SLW EVALUATION

In order to assess the potential for precipitation enhancement via cloud seeding CSEA was used to analyze cloud and environmental properties over New Mexico during a very dry year (Oct. 2002-Sep. 2003) and a very wet year (Oct. 2004-Sep. 2005) according to northern New Mexico river stream flow data (Shaull et al., 2008). There was a 48% increase in estimated cloud SLW during the wet period. The images in Figure 10 show the spatial distribution of the estimated cloud SLW in a rectangular region bounding the state of New Mexico for the two annual periods along with the 18.5 km resolution DEM. The color shading shows the relative cloud SLW mean values across the state. For instance, cloud SLW appears greater in the southern mountainous regions relative to the rest of the state during the 2002-03 year. This only means that the difference in estimated cloud SLW between the northern and southern regions of the state was greater in the latter annual period. Cloud SLW corresponds well with higher terrain as one would expect.

Further analysis was focused on a 1° x 1° region centered on Taos, NM, shown by the red boxes in the images of Figure 10. A smaller area was chosen so that local environmental effects could be assessed, and the Taos region, in particular, due to its location near the maximum estimated cloud SLW in both annual periods. Figure 11 shows the seasonal changes in the location of estimated cloud SLW over the Sangre de Cristo Mountains shown as the high elevation regions in the DEM (right image). This data corresponds to the area inside the red boxes in Figure 10. It is apparent that the estimated cloud SLW is concentrated on the west slopes of the mountains during the winter, but during the summer months it spreads out and shifts towards the eastern side of the range. This is consistent with the general shift in the mid-tropospheric wind patterns over the area.

Figure 12 shows the monthly total estimated cloud SLW mass in kilograms inside the northern NM AOI for both annual periods. Note that SLW was estimated for the cloud temperature range between 0° C and -40°C, but this exercise could be performed for any cloud temperature range desired. In most of the months larger amounts of cloud SLW were estimated during the wetter period. The largest difference between the wet and dry years occurred during the fall and winter months when precipitation generally occurs from mid-latitude storms steered by the polar jet stream.

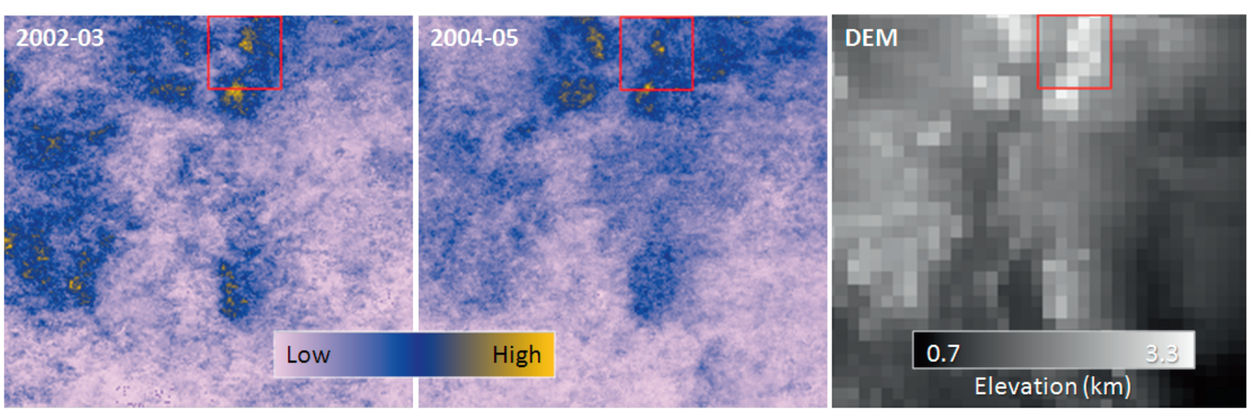

Figure 10: Mean estimated cloud SLW over the state of New Mexico for the annual periods 2002-03 (left) and 2004-05 (center), with the 18.5 km resolution Digital Elevation Map (right).

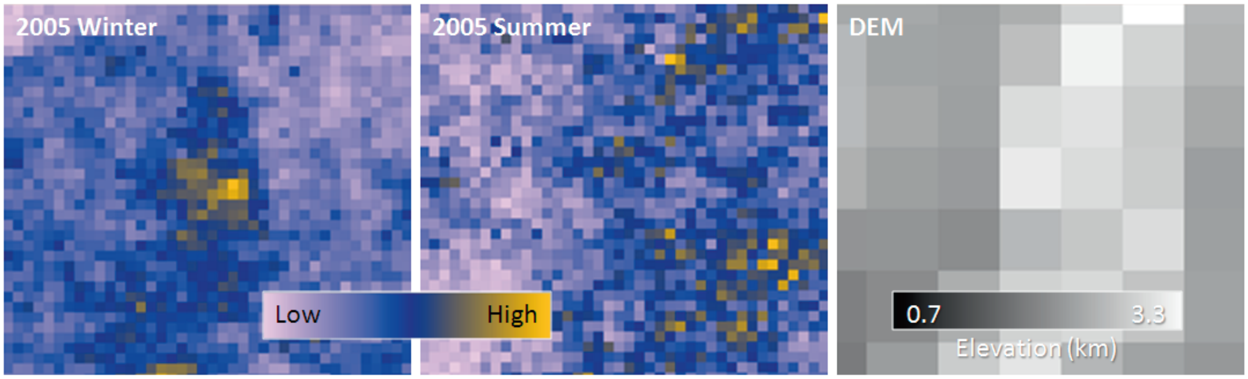

Figure 11: Mean estimated cloud SLW over the Sangre de Cristo Mountains in northern New Mexico for the winter (left) and summer (right) seasons of 2005, with the 18.5 km resolution Digital Elevation Map (right).

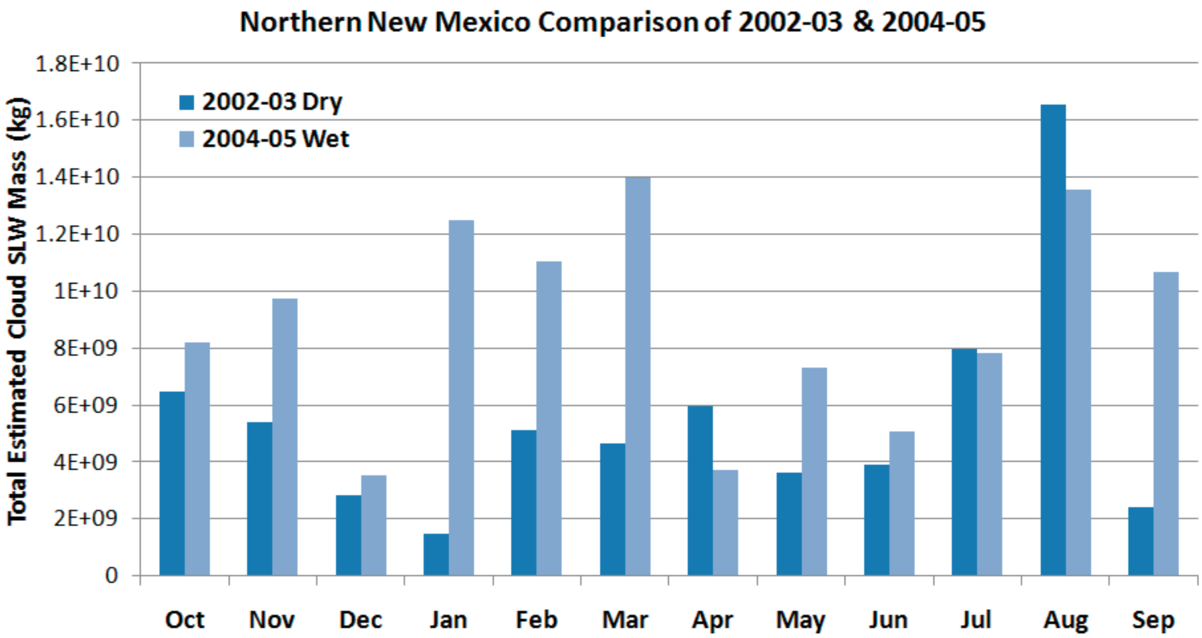

Figure 12: Monthly cloud SLW totals over Northern New Mexico during both dry and wet years.

To further investigate the potential cause for the increase in precipitation and estimated cloud SLW during the 2004-05 year, cloud and environmental properties from the northern New Mexican AOI were examined. The percent change from the 2002-03 to the 2004-05 winter periods (Nov. – Apr.) of the most important properties are plotted in Figure 13. Total precipitation (determined by ground measurements) increased by nearly 40% as suggested by the increase in stream flow, as did the number of days with measurable precipitation. Cloud SLW nearly doubled in the wet year despite reduced mean cloud thickness. Cloud coverage slightly increased, but not at the same level as the cloud SLW. The annual differences in mean cloud top temperature, optical depth and effective particle radius (r_e) were all less than 4%. The mean MODIS CWP did increase by nearly 20% in the wet year. The combination of more cloud water and higher cloud coverage along with a slightly higher mean cloud top temperature around -36°C seemed to positively influence the estimation of cloud SLW a great deal. By putting more clouds in a higher temperature range the cloud liquid water parameterization scheme likely assigned a much greater amount to the liquid state. Although algorithm sensitivity to cloud top temperature has yet to be investigated, the algorithm did show great sensitivity to both the MALR assumption and the cloud liquid water fraction parameterization due to cloud temperature and thermodynamic phase assignments. In addition, it was found that the estimated cloud SLW standard deviation was 70% greater during the wet annual period than the dry period indicating that large cloud SLW events could have greatly influenced the annual cloud SLW budget during the latter period. Precipitation was not highly correlated to estimated cloud SLW during either period (0.09 and 0.12, respectively), although it showed higher correlation (0.66) during the winter of 2007 that was assessed separately.

NCEP reanalysis data were sampled daily near the time that the satellite data was taken. These data consisted of air temperature, relative humidity, wind speed, and wind direction at 17 pressure levels. The wet year showed higher mean 700 mb relative humidity, as well as a greater number of days with a mid-tropospheric westerly wind. Interestingly, very little difference was seen in atmospheric temperature with only a minor increase in 700 mb and 500 mb temperatures. This indicates that a moister lower atmosphere with a higher number of westerly wind events may provide the conditions for increased precipitation in this region, especially for western mountain slopes due to their inherent lifting mechanism. It also shows the possibility that large increases in cloud SLW may occur for smaller positive changes in cloud coverage, cloud water content, humidity, and wind direction. From all of the NCEP environmental properties derived over the state of New Mexico during both years, the 700-500 mb relative humidity correlated best, although not strongly, with estimated cloud SLW giving values just above 0.5.

5. SUMMARY

An automated algorithm that estimates cloud super-cooled liquid water (SLW) content has been developed for the purpose of weather modification assessment for several small businesses in the state of New Mexico. The algorithm specifically relies on several MODIS derived cloud products as well as a parameterized vertical cloud thickness, temperature, and liquid water fraction. An initial long period trend analysis of potential cloud SLW has been performed for two recent extreme annual precipitation periods over the state of New Mexico. Estimated cloud SLW maximums were identified near mountainous regions across the state with the northern Sangre de Cristo Mountains around Taos, NM showing maximum values in both periods. Cloud SLW was estimated throughout the period, but the largest difference between the two years occurred during the winter months. Much of the summertime estimated cloud SLW likely occurred from convective cloud which is the dominate cloud type during the warm, moist summer season. At present, the algorithm cannot identify specific cloud types. It was found that statewide there was a nearly 50% increase in the estimated cloud SLW between the wet year and the dry period, and in a northern portion of the state the estimated cloud SLW nearly doubled. Further analysis was focus on a 1° x 1° region centered over the Taos region but contained both sides of the local mountainous area. From analysis of other cloud and environmental properties in this area-of-interest, it was discovered that only modest changes cloud coverage, cloud water content, and other bulk cloud properties accompanied this

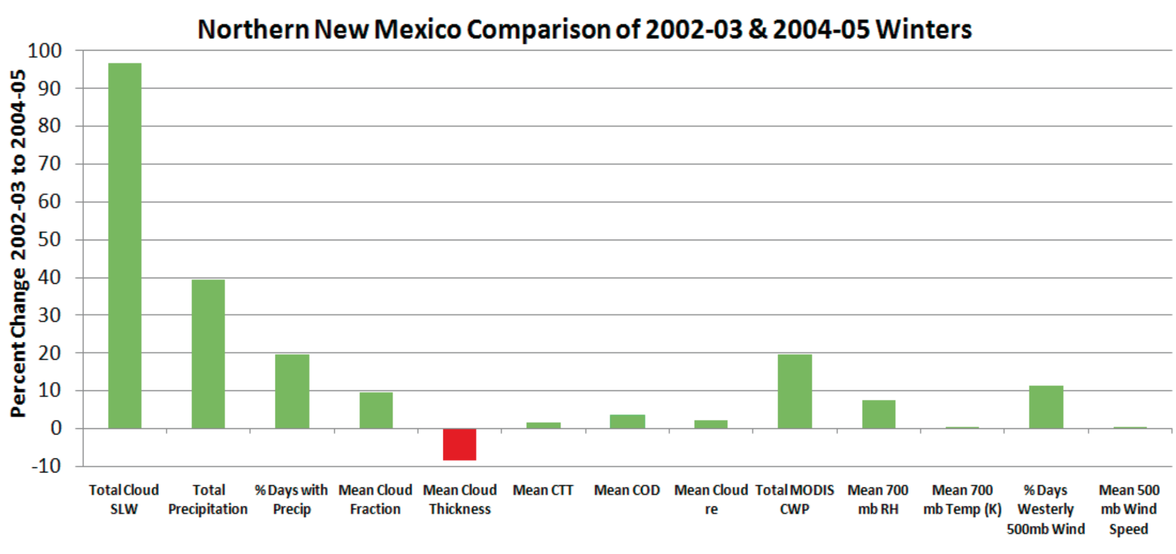

Figure 13: Percent change of important cloud and environmental properties between the dry (2002-03) and wet (2004-05) years.

large cloud SLW estimation increase. This likely resulted because the algorithm is very sensitive to the parameterization of the cloud moist adiabatic lapse rate and liquid water fraction which appeared to turn modest increases in cloud top temperature and cloud water path into a large potential cloud SLW increase. NCEP reanalysis data also showed that the wet year was associated with slightly greater lower-to-mid tropospheric humidity and a greater number of days in which the prevailing upper level wind was from the west.

Algorithm sensitivity analysis to scientific constants and parameterizations was performed which identified up to 30% variation in the resulting cloud SLW estimates for realistic variations of these parameters. The algorithm is directly affected by the MODIS CWP uncertainty which was derived to be about 30% with a standard deviation of 18% for clouds over New Mexico during the two year period. It was determined that the algorithm was likely to produce cloud SLW estimations within a factor of two of the true value given these uncertainties. Comparisons of the algorithm cloud SLW results with other data sources were made to verify that the results were realistic and agreed within the large approximated uncertainty bounds. Ground-based data from NSA-ARM site provided accurate cloud liquid water and cloud base height which were used together with Barrow soundings to ascertain cloud base temperatures in order to verify the presence of cloud SLW. In all cases, cloud base temperatures were below freezing which guaranteed the presence of super-cooled liquid water. Algorithm derived cloud SLW compared well to the ground measurements on average despite substantial daily differences. These differences were expected to a certain degree because of the large uncertainties associated with satellite derived cloud water content, especially large in polar data. The cloud base temperatures derived from the sounding data compared well with the extrapolated algorithm values. The algorithm was shown to overestimate cloud base height, by underestimating cloud thickness, on average by 930 meters. Algorithm derived cloud SLW concentration values and temperatures compared very well to *in-situ* aircraft measurements taken from two 3-minute flights during the ISDAC field campaign over the north slope of Alaska. Lastly, algorithm results were compared to CloudSat, space-based radar derived cloud top height, optical depth, thickness and total water column amount from 40 minutes of continuously collected data. Since all mean algorithm single layer cloud properties were lower than the corresponding CloudSat values, it is surmised that the algorithm may be underestimating cloud SLW due to the insensitivity of the passive cloud products to the lower cloud regions.

The algorithm remains limited in its ability to ascertain accurate conditions for cloud seeding since it only assesses theoretical temperature and liquid water fractions inside clouds and cannot depict important criteria needed for successful precipitation enhancement such as ice supersaturation and water vapor transport. Still, several algorithm enhancements would improve the accuracy of the algorithm's cloud SLW estimates. The development of a robust cloud typing methodology that would rely on new MODIS derived cloud phase algorithms, cloud height, and optical depth to classify clouds by altitude and convective nature would provide a better initial screening process as well as a precursor for separate cloud thickness parameterization schemes that are tailored to specific cloud types. Better vertical cloud temperature profiles could be produced that would be defined as a function of water content, temperature and geographical location. A great deal of improvement lies in a more accurate derivation of CWP based on the variation in the cloud effective particle radius with height. Chen et al. (2008) showed that a large difference existed in vertical cloud particle profiles between non-drizzling and drizzling stratiform cloud. Utilizing the standard MODIS derived effective particle radius (which employs the particle size sensitivity of the 2.1 μm band) together with the effective radius difference (which differences the size retrieval from the 3.7 μm band and the standard result) should provide a measure of the vertical effective cloud particle size. This occurs due to the cloud particle absorption differences at the two wavelengths; with the retrieval using the 3.7 μm band being sensitive only to the cloud top and the 2.1 μm band retrieval providing information further below cloud top (Platnick et al., 2003). Improved sensing of vertical cloud particle size distributions using MODIS calibrated radiances has been demonstrated for cirrus clouds by Wang et al. (2009). If applicable to mixed phase clouds this should provide more accurate cloud CWP derivations.

The simple parameterization of cloud liquid water fraction based solely on temperature can also be improved. In this study it served as a plausible method for defining possible cloud SLW. For more accurate retrievals increased knowledge of the cloud microphysical properties will have to be determined. For example, Wang and Wu (2010) suggest the importance of three criteria for the determination of potential artificial cloud seeding locales: ice supersaturation, accumulated water vapor within a below freezing temperature layer, and the vertical transport of water vapor. Using the high resolution MM5 mesoscale model they can potentially use forecasts of these properties to predict regions where the conditions are ripe for cloud seeding. Remote measurements must still be used to confirm model data and validate assumptions. For historical evaluations such as was provided here, NCEP reanalysis humidity and wind data along with terrain maps could be exploited as input for ambient water vapor and horizontal transport.

At the present time, the CSEA algorithm is temporally limited by the similar sun-synchronous daytime overpass times of the MODIS sensors which occur around 10:30 am and 1:30 pm local time for the Terra and Aqua satellites, respectively. The Visible Infrared Imager Radiometer Suite (VIIRS) sensors of the new Joint Polar Satellite System (JPSS) and Defense Weather Satellite System (DWSS) programs will have the capability of reproducing the important MODIS cloud products needed for the CSEA algorithm at some time in the future (Hutchison et al., 2005). Unfortunately, these sensors are not likely to be ready for launch until 2015 and 2018, respectively. The JPSS satellites will replace the MODIS satellites, but the first DWSS satellite is set to orbit at 5:30 am which along with the JPSS payloads will increase the number of daytime collections and provide information pertinent to the study of daytime cloud property variability. A more interesting option may be to modify the algorithm to accept Geostationary Operational Environmental Satellites (GOES) cloud products (Turk et al., 1998) including cloud liquid water (Greenwald and Christopher, 2000). These more continuous datasets would provide much better assessment of daily variations in cloud SLW as indicated by past studies concentrated on bulk cloud properties (Greenwald and Christopher, 1999). Lastly, retrieval of vertical and column cloud properties are inherently difficult from passive satellite sensors. Currently, spaceborne environmental radar and lidar systems which are markedly more sensitive to the vertical cloud structure and imbedded supercooled liquid water layers (Hogan et al., 2004) do not scan and, therefore, cannot perform large area coverage. Still, these early systems do exist in space and coincide with broad area coverage passive scanning sensors in a single line-of-sight along the satellite orbit and can provide valuable corrections to passive satellite data, at least in the area of coincident data.

Future work will include the previous described algorithm and data enhancements but will be closely linked to other remote sensing instruments that can provide accurate retrievals of cloud properties such as liquid water content, temperature, and cloud particle size for algorithm validation, improved parameterization, and cloud SLW evaluation. Comprehensive evaluation of data above well instrumented ground sites such as the DOE's Atmospheric Radiation Measurement sites should dramatically help. Possible sites on both the western and eastern slopes of the northern New Mexico Mountains are being explored as well to better fulfill the interests of the state stakeholders. The mode of operation would likely consist of either two fully instrumented sites or a move from an established site on the western slopes during the winter to a site on the eastern side for the summer coincident with the estimated maximum cloud SLW identified in this study.

Acknowledgements: This work was funded through the New Mexico Small Business Assistance (NMSBA) program. The NMSBA Programs at Sandia and Los Alamos National Laboratories were created in response to New Mexico's Laboratory Partnership with Small Business Tax Credit Act. The authors would like to thank Dan Breed for making the University of Wyoming radiometer data available to us.

REFERENCES

Boudala, F.S., G.A. Isaac, S.G. Cober and Q. Fu, 2004: Liquid fraction in stratiform mixed-phase clouds from *in situ* observations. *Q. J. Roy. Meteorol. Soc.*, **130**, 2919–2931, doi: 10.1256/qj.03.153.

Boe, B.A., 2008: Operational aspects of the Wyoming Weather Modification Pilot Project: an Update. 17th Joint AMS/WMA Conference on Planned and Inadvertent Weather Modification and WMA Annual Meeting, 20-25 April 2008, Westminster, Colorado, USA.

Chakrapani, V., D.R. Doelling, A.D. Rapp, and P. Minnis, 2002: Cloud thickness estimation from GOES-8 satellite data over the ARM SGP site. In *Proceedings of the Twelfth Atmospheric Radiation Measurement (ARM) Science Team Meeting*, ARM-CONF-2002.

Chen, R., F-L. Chang, Z. Li, R. Ferraro, and F. Weng, 2007: Impact of the vertical variation of cloud droplet size on the estimation of cloud liquid water path and rain detection. *J. Atmos. Sci.*, **64**, 3842-3853, doi: 10.1175/2007JAS2126.1.

Chen, R., R. Wood, Z. Li, R. Ferraro, and F.-L. Chang, 2008: Studying the vertical variation of cloud droplet effective radius using ship and spaceborne remote sensing data., *J. Geophys. Res.*, **113**, D00A02, doi:10.1029/2007JD009596.

Chylek, P., S. Robinson, M.K. Dubey, M.D. King, Q. Fu, and W.B. Clodius, 2006: Comparison of near-infrared and thermal infrared cloud phase detections. *J. Geophys. Res.*, **111**, D20203, doi: 10.1029/2006JD007140.

Cooper, W.A., and R.P. Lawson, 1984: Physical interpretation of results from the HIPLEX-1 experiment. *J. Climate Appl. Meteor.,* **23,** 523–540.

Cotton, W.R., and R.A. Pielke, 1995: Human Impacts on Weather and Climate. Cambridge Univ. Press, 288 pp.

Cotton, W.R, 2009: Weather and Climate Engineering, Clouds in the Perturbed Climate System: The Relationship to Energy Balance. *Atmospheric Dynamics and Precipitation*, MIT Press ISBN 978-0-262-01287-4, **15**, 339-367.

Doutriaux-Boucher, M. and J. Quaas, 2004: Evaluation of cloud thermodynamic phase parametrizations in the LMDZ GCM by using POLDER satellite data. *Geophys. Res. Lett.,* **31**, L06126, doi:10.1029/2003GL019095.

Geerts, B., Q. Mio, Y. Yang, R. Rasmussen, and D. Breed, 2010: An airborne profiling radar study of the impact of glaciogenic cloud seeding on snowfall from winter orographic clouds. *J. Atmos. Sci*., **67** (10), 3286-3302, doi: 10.1175/2010JAS3496.1.

Greenwald, T.J., and S.A. Christopher, 1999: Daytime variation of marine stratocumulus microphysical properties as observed from geostationary satellite. *Geophys. Res. Lett.,* **26,** 1723–1726.

Greenwald, T.J. and S.A. Christopher, 2000: The GOES I-M Imagers: New tools for studying microphysical properties of boundary layer stratiform clouds. *Bull. Amer. Meteor. Soc.*, **81**, 2607-2619.

Han, Q., W.B. Rossow, J. Chou, and R.W. Welch, 1998: Global survey of the relationships of cloud albedo and liquid water path with droplet size using ISCCP. *J. Climate,* **11,** 1516–1528.

Heggli, M.F. and R.M. Rauber, 1988: The characteristics and evolution of supercooled water in wintertime storms over the Sierra Nevada: A summary of microwave radiometric measurements taken during the Sierra Cooperative Pilot Project. *J. Appl. Meteor.*, **27**, 989–1015, doi: 10.1175/1520-0450.

Heymsfield, A.J., M.L. Miloshevich, A. Slingo, K. Sassen, and D. Starr, 1991: Observational and theoretical study of high supercooled altocumulus. *J. Atmos. Sci.*, **48**, 923–945.

Heymsfield, A.J. and M.L. Miloshevich, 1993: Homogeneous ice nucleation and supercooled liquid water in orographic wave clouds. *J. Atmos. Sci.*, **50**, 2335–2353, doi: 10.1175/1520-0469(1993)050.

Heymsfield, A.J., Patrick C. Kennedy, S. Massie, C. Schmitt, Z. Wang, S. Haimov, A. Rangno, 2010: Aircraft-Induced Hole Punch and Canal Clouds: Inadvertent Cloud Seeding. *Bull. Amer. Meteor. Soc.*, **91**, 753-766, doi: 10.1175/2009BAMS2905.

Hogan, R.J., M.D. Behera, E.J. O'Connor, and A.J. Illingworth, 2004: Estimate of the global distribution of stratiform supercooled liquid water clouds using the LITE lidar. *Geophys. Res. Lett.*, **31**, L05106, doi:10.1029/2003GL018977.

Horvath, A. and S. Chellappan, 2009: Evaluation of passive satellite remote sensing of cloud liquid water. Geoscience and Remote Sensing Symposium, 2009 IEEE International, IGARSS 2009 , vol.3, no., pp.III-1015-III-1018, 12-17 July 2009, doi: 10.1109/IGARSS.2009.5417950.

Huggins, A.W., 2009: Summary of studies that document the effectiveness of cloud seeding for snowfall augmentation, *J. Weather Mod.*, **41**, 119-126.

Hutchison, K., J. Roskovensky, J. Jackson, A. Heidinger, M. Pavolonis, and R. Frey, 2005: Automated cloud detection and classification of data collected by the Visible Infrared Imager Radiometer Suite (VIIRS). *Int. J. Remote Sens.,* **26**, 21, 4681-4706.

King, M.D., S.-C. Tsay, S. Platnick, M. Wang, and K.N. Liou, 1998: Cloud retrieval algorithms for MODIS: Optical thickness, effective particle radius, and thermodynamic phase. Available at: http://modis-atmos.gsfc.nasa.gov/MOD06_L2/atbd.html.

Korolev, A.V., G.A. Isaac, J.W. Strapp, S.G. Cober and H.W. Barker, 2007: *In situ* measurements of liquid water content profiles in midlatitude stratiform clouds. *Q. J. Roy. Meteorol. Soc.,* **133**, 1693–1699.

Liu, S., G. Heygster, and S. Zhang, 2010: Comparison of CloudSat cloud liquid water paths in arctic summer using ground-based microwave radiometer. *J. Ocean Univ. China* (*Oceanic and Coastal Sea Research*)*,* **9** (4), 333-342, doi: 10.1007/s11802-010-1740-y.

Menzel, W.P., R.A. Frey, B.A. Baum, 2010: Cloud top properties and cloud phase - Algorithm Theoretical Basis Document, available at: http://modis-atmos.gsfc.nasa.gov/MOD06_L2/atbd.html.

Minnis, P., W.L. Smith, Jr., D.P. Garber, J.K. Ayers, and D.R. Doelling, 1995: Cloud properties derived from GOES-7 for Spring 1984 ARM Intensive Observing Period using Version 1.0.0 of ARM satellite data analysis program. NASA RP 1366, pp.58.

Minnis, P., W.L. Smith, L. Nguyen, F.-L. Chang, D. Spangenberg, R. Palikonda, C. Yost, and M. Khaiyer, 2008: Detection of aircraft icing conditions using an enhanced cloud retrieval method applied to geostationary satellite data. Presented at *the American Meteorology Society 13th Conference on Aviation, Range, and Aerospace Meteorology*, New Orleans, LA, January 2008.

Nasiri, S.L., and B.H. Kahn, 2008: Limitations of bispectral infrared cloud phase determination and potential for improvement. *J. Appl. Meteor. Climatol*., **47**, 2895-2910, doi: 10.1175/2008JAMC1879.1.

Platnick, S., M.D. King, S.A. Ackerman, W. Paul Menzel, B.A. Baum, and R.A. Frey, 2003: The MODIS cloud products: Algorithms and examples from Terra. *IEEE Trans. Geosci, Remote Sens.,* **41**, 459-473.

Platnick, S., R. Pincus, B. Wind, M. D. King, M. Gray, and P. Hubanks, 2004: An initial analysis of the pixel-level uncertainties in global MODIS cloud optical thickness and effective particle size retrievals, Passive Optical Remote Sensing of the Atmosphere and Clouds IV. *Proc. of SPIE,* Vol. **5652**, doi: 10.1117/12.578353.

Remer, L.A., Y.J. Kaufman, D. Tanré, S. Matto, D.A. Chu, J.V. Martins, R.-R. Li, C. Ichoku, R.C. Levy, R.G. Kliedman, T.F. Eck, E. Vermote, and B.N. Holben, 2005: The MODIS aerosol algorithm products and validation. *J. Atmos. Sci*., **62** (4), 947-973.

Remer, L.A., D. Tanré, and Y.J. Kaufman, 2006: Algorithm for remote Sensing of Tropospheric Aerosol from MODIS, available at: http://modis.gsfc.nasa.gov/data/atbd/atbd_mod02.pdf

Rosenfeld, D., 2000: Suppression of rain and snow by urban air pollution. *Science,* **287,** 1793–1796.

Shaull, D.A., D. Ortiz, M.R. Alexander, and R.P. Romero, 2008: Surface water data at Los Alamos National Laboratory 2000 - 2008 water year*, LA-14131-PR* Progress Report Los Alamos National Laboratory, Los Alamos NM.

Spangenberg, D.A., P. Minnis, M.D. Shupe ,and M.R. Poellot, 2006a: Retrieval of cloud phase over the Arctic using MODIS 6.7 – 12 μm data. In proceedings of the AMS Fourteenth Conference Satellite Meteorology and Oceanography, Atlanta, GA, January-February, 2006.

Spangenberg, D.A., P. Minnis, S. Sun-Mack, M.D. Shupe, and M.R. Poellot, 2006b: Characterization of mixed-phase clouds during Mixed-phase Arctic Cloud Experiment from satellite, ground-based, and *in-situ* data. Presented at *the Sixteenth ARM Science Team Meeting Proceedings*, Albuquerque, NM, March 2006.

Turk, J., J. Vivekanandan, T. Lee, P. Durkee, and K. Nielsen, 1998: Derivation and applications of near-infrared cloud reflectances from GOES-8 and GOES-9. *J. Appl. Meteor.,* **37,** 819–831.

Twomey, S., 1977: The influence of pollution on the shortwave albedo of clouds. *J. Atmos. Sci.*, **34**, 1149–1152, doi: 10.1175/1520-0469(1977)034.

Wang, X., K.N. Liou, S.S.C. Ou, G.G. Mace, and M. Deng, 2009: Remote sensing of cirrus cloud vertical size profile using MODIS data. *J. Geophys Res.*,**114**, D09205, doi: 10.1029/2008DJ011327.

Wang, Y. and W. Wu, 2010: A new method in determining potential region of precipitation enhancement above coastal land. *J. Ocean Univ. China* (*Oceanic and Coastal Research*), **9**, 209-316.

Wentz, F.J., 1997: A well-calibrated ocean algorithm for special sensor microwave/imager, *J. Geophys. Res.*, **102** (C4), 8703–8718, doi:10.1029/96JC01751.

Xing, Y, Dai Jin, L. Hengchi, X. Xiaohong, F. Peng, C. Zhengqi, D. Changhui, and W. Yong, 2005: Physical effect of cloud seeding revealed by NOAA satellite imagery. *Chinese Sci. Bull.,* **50** (1), 44-51.